A COMPARISON OF SUBGRID SCALE MODELS FOR LARGE EDDY SIMULATION OF A CO-ANNULAR SWIRLING FLOW FIELD

Jessica Gullbrand*
Dept. of Heat and Power Engineering/Fluid Mechanics,
Lund Institute of Technology, SE-221 00 Lund, Sweden

Johan Revstedt†
Dept. of Heat and Power Engineering/Fluid Mechanics,
Lund Institute of Technology, SE-221 00 Lund, Sweden

Laszlo Fuchs‡
Dept. of Heat and Power Engineering/Fluid Mechanics,
Lund Institute of Technology, SE-221 00 Lund, Sweden

ABSTRACT

Large Eddy Simulation (LES) of an incompressible, turbulent, co-annular swirling flow field have been performed in order to compare the influence of different subgrid scale (SGS) models. Two models were investigated, an implicit model and a stress similarity model. In the simulations using the implicit approach, no explicit SGS model was used. For the stress similarity model, similar behaviour between the resolved and unresolved stresses was assumed. The results from the simulations are compared with experimental data for mean velocities and turbulence intensities.

INTRODUCTION

Swirling motion of the flow field is applied in many practical applications. Flame stabilisation in a combustor can be achieved by introducing a swirling motion into the inlet flow stream. Another feature that is influenced by a swirling motion is the mixing rate between species. The mixing rate in the flow field is enhanced when the motion is introduced. Hence swirling flows are of great engineering interest and it is important to be able to predict and model these types of flows. Swirling flows are difficult to simulate with Reynolds averaged Navier-Stokes (RANS) models, therefore LES is a natural approach.

It is well known that eddy viscosity based (RANS) turbulence models have difficulties with flows which are highly curved such as swirling flows and that LES does not suffer from this shortcoming. LES resolves all the large length scales of the turbulence and only the small ones are modelled. The small scales are of universal character and therefore lend themselves to local and generally valid models. The model should predict the influence of the small scales on the large ones and also the interaction between the small unresolved length scales.

The interest in LES and the models for the small scales, the subgrid scales (SGS), has increased in recent years. Many models have been proposed, modified and tested. Comparisons between some proposed SGS models have been made and most of them have been applied on homogeneous isotropic turbulence. SGS models have been compared in papers by Clark *et al.*(1979), Fureby *et al.*(1997) and Menon *et al.*(1996). Their comparisons were also made by using data from Direct Numerical Simulations (DNS). The drawback is that DNS data is only available for low Reynolds number flows and the behaviour of the SGS models can be quite different for

*Ph.D. student
†Ph.D. student
‡Professor

large Reynolds numbers. In fact LES should perform best for large Reynolds numbers, rather than for low ones.

This paper compares and evaluates two SGS models with experimental data for a highly swirling co-annular flow field. The objective was to compare SGS models in a demanding environment with more practical applications. The flow field is of relatively high Reynolds number and therefore, no DNS data is available for this flow. The evaluation of the models is made with experimental data from Ribeiro and Whitelaw.

GOVERNING EQUATIONS

The governing equations for LES are the space filtered continuity equation and Navier-Stokes equations for an incompressible flow. A filter function $\overline{G}$ with the filter width Δ is applied to the flow variable ϕ resulting in the filtered flow variable $\overline{\phi}$, according to

$$\overline{\phi(x,t,\Delta)} = \int_{-\infty}^{\infty} \overline{G}(x-x',\Delta)\phi(x',t)dx'.$$

This filter is applied to the unfiltered governing equations and the filtered continuity equation and Navier-Stokes equations are obtained.
The continuity equation becomes

$$\frac{\partial \overline{u}_i}{\partial x_i} = 0, \tag{1}$$

and the Navier-Stokes equations are

$$\frac{\partial \rho \overline{u_i}}{\partial t} + \frac{\partial \rho \overline{u}_i \overline{u}_j}{\partial x_j} = -\frac{\partial \overline{p}}{\partial x_i} + \mu \frac{\partial}{\partial x_j}\frac{\partial \overline{u}_i}{\partial x_j} - \frac{\partial \tau_{ij}}{\partial x_j}. \tag{2}$$

ρ denotes the density, t is the time, p is the pressure and μ is the laminar viscosity. u_i is the velocity vector and x_i, the space coordinates. The filting divides the flow field components into two different groups. The first group contains the eddies that are larger than the filter width and therefore, are fully resolved. The second group consists of the small unresolved eddies. τ_{ij}, which is the subgrid scale stress tensor, represents the interaction between the small scales and the resolved and unresolved eddies. The definition of the SGS tensor is

$$\tau_{ij} = \rho(\overline{u_i u_j} - \overline{u}_i \overline{u}_j). \tag{3}$$

The stress tensor cannot be expressed in terms of the filtered variables since it consists of the unknown term $\overline{u_i u_j}$ and therefore, it has to be modelled by an appropriate model.

Subgrid Scale Models

The goal of a SGS model is to provide a model expressing the SGS stress in terms of the resolved variables. Different SGS models have been proposed and they are based upon different assumptions how the resolved flow variables influence the SGS stress. The model should account for some basic features of turbulence. An essential factor is the energy cascade, leading to dissipation on small scales, and energy transfer among different, resolved/unresolved, scales. One of the first proposed models was the Smagorinsky model (1963). It is an eddy viscosity type model. The model is absolutly dissipative which means that it can account for the viscous dissipation of the unresolved scales. The energy transfer in the other direction, from small to large eddies, is called back-scatter and occurs also in turbulent flow fields. The drawback of the Smagorinsky model is that it cannot account for this phenomena.

Two SGS models that are able to predict back-scatter are applied to the swirling flow field. The models are an implicit model and a stress similarity model. The models have been chosen because of their abilities to predict back-scatter, and also since they can be easily implemented in the code, while requiring only small amount of additional computational work.

Implicit Model. The implicit model (IMP) employes no explicit SGS model. The truncation error due to the discretization scheme can act as a SGS model. These terms contain a dissipative part while it allow to some extent, not physically related, back-scatter. In the simulations, a third order scheme proposed by Rai and Moin (1991) is used for the convective terms and higher order schemes are used for the other terms. The third order term is the largest term in the truncation error and it can be expressed as

$$\tau_{ij,j} = \frac{1}{4}\rho \sum_{j=1}^{3} |\overline{u}_j| \Delta x_j^3 \frac{\partial^4 \overline{u}_i}{\partial x_j^4}. \tag{4}$$

Δx_j is the size of the cell in the j-direction. This term is used to estimate the value on the truncation error and thereby the contribution of the implicit model.

Stress Similarity Model. The stress similarity model (SSM) is based upon similar behaviour between the resolved and unresolved stresses. The resolved stresses are calculated by applying a second filter function with wider filter width on the resolved flow field. The SSM proposed by Liu *et al.*(1994) is

$$\tau_{ij} - \frac{1}{3}\delta_{ij}\tau_{kk} = C_L \rho(\widehat{\overline{u}_i \overline{u}_j} - \widehat{\overline{u}}_i \widehat{\overline{u}}_j). \tag{5}$$

The model was shown not to dissipate an enough amount of energy and therefore, it was suggested to be used as a mixed model, Liu *et al.*(1994). The mixed model is a linear combination of the SSM and the Smagorinsky model.

In the simulations, a mixed model has been used. The difference between Liu *et al.*'s mixed model and the applied is that the Smagorinsky model has been replaced with the numerical dissipation, the implicit model. Therefore, the expression for the applied model can be written,

$$(\tau_{ij} - \frac{1}{3}\delta_{ij}\tau_{kk})_{,j} = (C_L\rho(\widehat{\overline{u}_i\overline{u}_j} - \widehat{\overline{u}}_i\widehat{\overline{u}}_j))_{,j} + \frac{1}{4}\rho\sum_{j=1}^{3}|\overline{u}_j|\Delta x_j^3\frac{\partial^4\overline{u}_i}{\partial x_j^4}. \quad (6)$$

The truncation error, the last term in equation (6), is not absolutely dissipative and thus both terms in the equation can provide back-scatter.

The two applied filter functions in equation (6) are a grid filter denoted by $\overline{\phi}$ and a Gaussian-type filter, $\widehat{\phi}$. The filter width of the Gaussian type of filter is twice as large as the grid filter, $\widehat{\Delta}/\Delta = 2$. The filter function for the wider filter can be expressed as $\frac{1}{6}(1,4,1)$, in one dimension.

NUMERICAL METHODS

The space discretization of the governing equations are performed on a uniform staggered Cartesian grid. The convective terms are discretized by a third order upwind scheme proposed by Rai and Moin (1991) and the other terms are discretized using a fourth order central difference scheme. A second order implicit scheme is applied for the time derivative. The discretized equations are solved iteratively by a multi-grid method and a distributed Gauss-Seidel algorithm is used for the coupling between pressure and velocity. More details about the numerical methods used in this code can be read in Bai and Fuchs (1992).

TEST CASE

The developing region of a co-annular swirling flow field was studied. The data for the air jet at atmospheric pressure was taken from Ribeiro and Whitelaw (1979). The air is supplied through two concentric pipes located in the wall. The diameter is 1.61 cm of the circular inlet and the inner and outer diameters of the co-annular inlet are 2.16 cm and 4.49 cm, respectively. The Reynolds number is 27 700 for the circular inlet and 53 900 for the co-annular. The flow through the co-annular inlet has a swirl number of 0.26.

NUMERICAL SIMULATIONS

The computational geometry is a three dimensional cubic box with the length of $12D$, where D is the largest diameter of the inlets. The inlets are symmetrically placed on one wall of the box. No-slip conditions are valid on this surface. The outlet is parallel to the inlet and the outlet condition is zero gradient of all dependent variables. In order to minimize the effect of the outlet conditions, the domain of interest is only the first half of the box in the streamwise direction. On all other surfaces symmetric boundary conditions, with zero gradients, are employed.

The mean velocity profiles for each inlet are given by the experiments and the inlet turbulence levels are estimated. The turbulence level at the inlets is simulated with white noise perturbations of 5 % of the magnitude of the inlet speed through the circular inlet and 17,5 % of the speed through the co-annular one.

The time step in the simulations is limited by the fact that the truncation error from the second order implicit scheme applied on the time derivative should not be larger than the error from the third order convective term.

The computational grid consists of three multi-grid levels and two local grid refinements. The size of the finest local grid is $6D$x$4D$x$4D$. The evolution of the flow field is of interest and therefore, the grid starts at the inlets and ends $6D$ downstream. The computational cells are cubic in shape and the number of cells are 120x80x80.

RESULTS

The results from the simulation using the two different SGS models, implicit and stress similarity model, are compared with experiments for mean velocities and turbulence intensities. In all the figures, the circles represent results from the experiments (EXP) and lines, results from the simulations. The results from the simulations using the implicit model (IMP) are represented by a solid line and stress similarity model (SSM) by a dashed line.

The energy spectra are also investigated at two different positions along the center-line axis. For this type of data, unfortunately, there exist no experimental data and the simulations are compared to each other.

Mean Velocities

The difference is large between the results from the simulation and experiments for the mean velocities. In figure 1, the mean velocities in the axial, tangential and radial direction are shown as a function of the radial distance from the center-axis. The position in the streamwise direction is $1.5D$ from the inlets. The figure shows some differences between the employed SGS models. The SSM shows a higher peak value than IMP in all directions.

The mean velocities in the axial direction for the simulations show the same profile as the experiments

further downstream. The same velocities as in the previous figure is shown at the position $6D$ from the inlets in figure 2. The difference between the simulated results are smaller, but there is still a large difference between the simulated and experimental results. In the graph for the mean axial velocity, it is noted that the mass flow in the simulations and experiments are not the same.

Along the center-axis, the mean axial velocity shows a greater dependence upon the SGS model, in figure 3, than along the radial direction. In the figure, the mean velocity for the SGS models differs in absolute value by the most 7 %, but the curves have approximately the same shape. The dips and peak of the profile from the experimental curve differs in location from the simulated ones.

Turbulence Intensities

The turbulence intensities are highly underpredicted when simulated results are compared with experiments. In figure 4, the turbulence intensities in the axial, tangential and radial direction are shown as a function of the radial distance from the center-axis at the position $1.5D$ from the inlets. The last graph in the figure shows the kinetic energy as a function of the radial distance. It is interesting to notice that the turbulence intensity for the SSM is higher than for IMP at $r = R$.

Further away from the inlets, the SSM shows lower turbulence intensities than IMP, in figure 5. In this figure, the same variables as in figure 4 are shown at a position $6D$ from the inlets. At this position, the peak shown in figure 4 has vanished and the turbulence intensities are lower for SSM than for IMP.

When the turbulence intensities are studied along the center-axis, it is clearly seen that the turbulence level in the inlets are wrongly defined in the simulations, figure 6. The fluctuating components as predicted by both SGS models grow somewhat differently but reach approximately the same level after $5D$.

Energy Spectra

The Eulerian time spectrum of the turbulent kinetic energy shows what length scales of the turbulence that are resolved in the simulations. Figures 7 and 8 show the kinetic energy spectra at point $1.3D$ and $5.5D$ from the inlets along the center-axis, respectively. The circles represent the results from the simulations using IMP and the crosses simulations using SSM. The solid line shows the slope of the decay in turbulent kinetic energy valid for isotropic turbulence. The turbulence in the swirling flow is most likely not isotropic, but the slope gives an indication of what length scales in the turbulence that are resolved in the simulations. In figure 7, it is shown that some large structures in the flow field exist.

The kinetic energy spectrum in figure 8 shows that there exist more length scales at this position ($5.5D$) than at the previous location ($1.3D$). This is an indication of that the flow field is, almost fully developed, turbulent at that location.

DISCUSSION AND CONCLUSIONS

Some of the discrepancies between the simulated and experimental mean velocity profiles and turbulence intensities are due to the way inlet turbulence is applied. In our calculations, this is done by applying a given level of random perturbations. The spectral composition of this inlet condition is of course not physical. Also, it is clear that while the high frequency components are dissipated, the lower frequencies has to be amplified to yield ultimate a turbulent flow field. This observation is supported by considering the turbulence intensities along the center-axis, figure 6. It is clearly seen that the inlet perturbations are small near the inlet. The figure also shows that the turbulence levels finally starts to grow to reach a certain level, approximately after $5D$ from the inlets. In figure 4, it seems that the SSM yields a quicker initial growth than the IMP. A remedy to this problem might be to use a long inlet tube where the flow is allowed to develop naturally. This would require an inlet tube of length of about 5-6 tube diameters.

The discrepancy between the different mass flows observed in figure 2 for mean axial velocity is most likely also due to the different turbulence levels in the simulations and experiments. The difference is due to entrainment of the surrounding air. In the experiments, the flow is already turbulent when it leaves the inlets and this results in a larger entrainment. In the simulations, the flow is not turbulent from the beginning. Instabilities starts to grow in the flow and finally it becomes turbulent. This is shown in the figures for the turbulent kinetic energy spectra. The number of existing length scales increase between the positions $1.3D$ to $5.5D$ along the center-axis, when figure 7 is compared with figure 8.

In summary, we conclude that due to difficulties in inlet conditions, a direct comparison between experiments and LES is not possible. It is also believed that the highly swirling flow problem is a good test case for SGS models, since the small effects of the unresolved scales can be seen also in the resolved, and the mean variables.

ACKNOWLEDGEMENT

This work is supported by the EC contract BRPR-CT95-0109 and from the CECOST research and grad-

uate school program. This supports are highly appreciated.

REFERENCES

Bai, X.S. and Fuchs, L., 1992, "Fast multigrid method for 3-D turbulent incompressible flows", *Int. J. Num. Meth. Heat Fluid Flow*, vol. 2, pp. 127-137.

Clark, R.A., Ferziger, J.H. and Reynolds, W.C, 1979, "Evaluation of subgrid-scale models using an accurately simulated turbulent flow", *J. Fluid Mech.*, vol. 91, pp. 1-16.

Fureby, C., Tabor, G., Weller, H.G. and Gosman, A.D., 1997, "A comparative study of subgrid scale models in homogeneous isotropic turbulence", *Phys. Fluids*, vol. 9, no. 5, pp. 1416-1429.

Liu, S., Meneveau, C. and Katz, J., 1994, "On the properties of similarity subgrid-scale models as deduced from measurements in a turbulent jet", *J. Fluid Mech.*, vol. 275, pp. 83-119.

Menon, S., Yeung, P.-K. and Kim, W.-W., 1996, "Effect of subgrid models on the computed interscale energy transfer in isotropic turbulence", *Comp. & Fluids*, vol. 25, no. 2, pp. 165-180.

Rai, M.M. and Moin, P., 1991, "Direct simulations of turbulent flow using finite difference schemes", *J. of Comp. Phys.*, vol. 96, pp. 15.

Ribeiro, M.M. and Whitelaw J.H., 1979, "Coaxial jets with and without swirl", *J. Fluid Mech.*, vol. 95, pp. 769-795.

Smagorinsky, J., 1963, "General circulation experiments with the primitive equations", *Mon. Weather Rev.*, vol. 91, pp. 99-166.

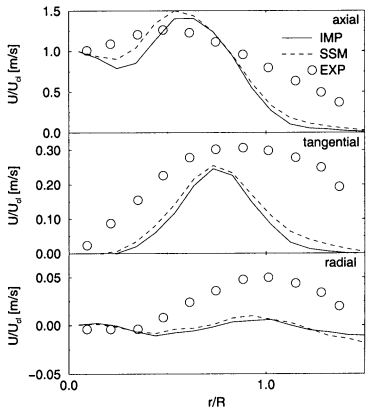

Figure 1: The normalised mean velocities in the axial, tangential and radial direction as a function of the normalised radius ($R = D/2$) at a position $1.5D$ from the inlets.

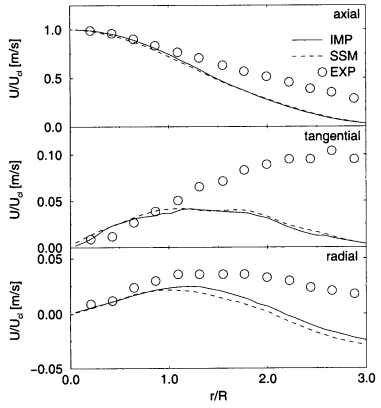

Figure 2: The normalised mean velocities in the axial, tangential and radial direction as a function of the normalised radius ($R = D/2$) at a position $6D$ from the inlets.

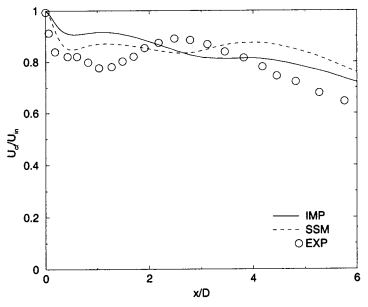

Figure 3: The normalised mean velocity in the axial direction along the center-axis of the swirling flow.

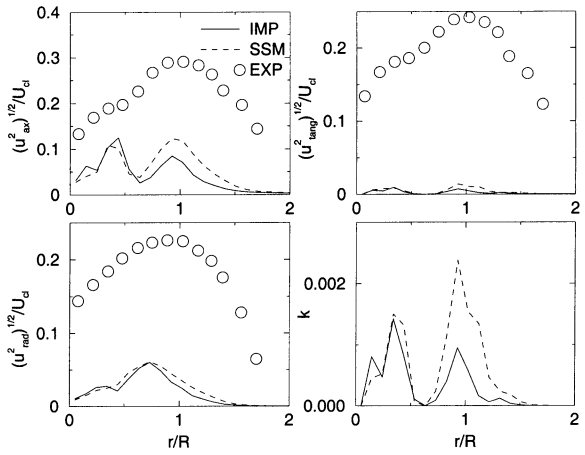

Figure 4: The normalised turbulence intensities in the axial, tangential and radial direction and the kinetic energy as a function of the normalised radius at a position $1.5D$ from the inlets. The kinetic energy is calculated according to $k = 0.5 * (u_{ax}^2 + u_{tang}^2 + u_{rad}^2)/U_{cl}^2$.

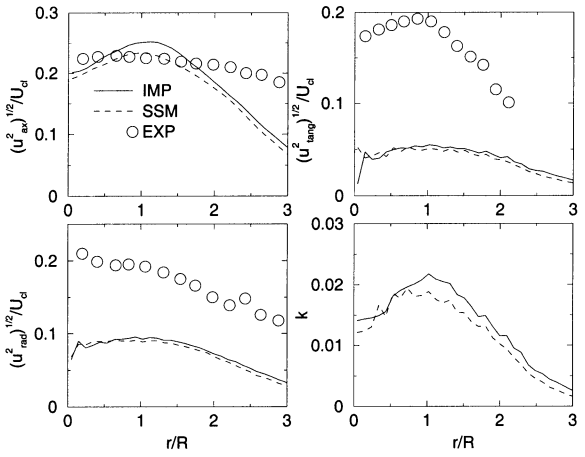

Figure 5: The normalised turbulence intensities in the axial, tangential and radial direction and the kinetic energy as a function of the the normalised radius at a position $6D$ from the inlets.

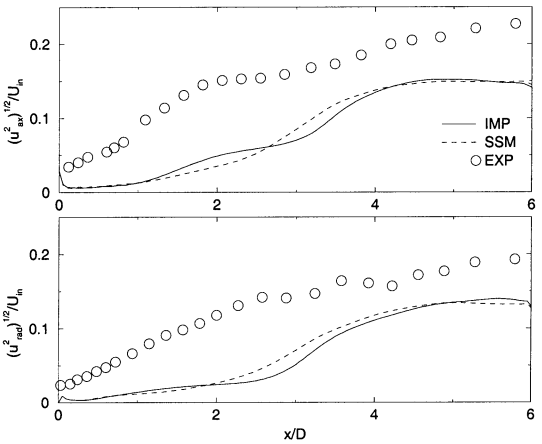

Figure 6: The normalised turbulence intensities in the axial and radial direction along the center-axis of the swirling flow.

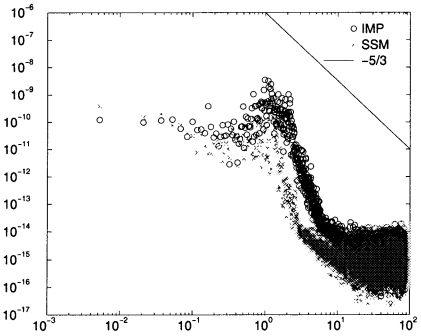

Figure 7: The kinetic energy spectra at a position $1.3D$ from the inlets along the center-axis.

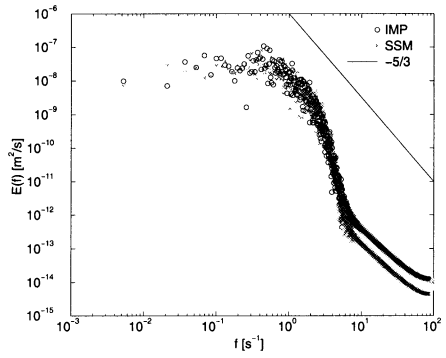

Figure 8: The kinetic energy spectra at a position $5.5D$ from the inlets along the center-axis.